Theory of chaos regularization of tunneling in chaotic quantum dots

Ming-Jer Lee,[1,*] Thomas M. Antonsen,[1] Edward Ott,[1] and Louis M. Pecora[2]
[1]*University of Maryland, College Park, Maryland 20742, USA*
[2]*Materials Physics and Sensors, U.S. Naval Research Laboratory, Washington, D.C. 20375, USA*
(Received 19 June 2012; published 21 November 2012)

Recent numerical experiments of Pecora *et al.* [Phys. Rev. E **83**, 065201 (2011)] have investigated tunneling between two-dimensional symmetric double wells separated by a tunneling barrier. The wells were bounded by hard walls and by the potential barrier which was created by a step increase from the zero potential within a well to a uniform barrier potential within the barrier region, which is a situation potentially realizable in the context of quantum dots. Numerical results for the splitting of energy levels between symmetric and antisymmetric eigenstates were calculated. It was found that the splittings vary erratically from state to state, and the statistics of these variations were studied for different well shapes with the fluctuation levels being much less in chaotic wells than in comparable nonchaotic wells. Here we develop a quantitative theory for the statistics of the energy level splittings for chaotic wells. Our theory is based on the random plane wave hypothesis of Berry. While the fluctuation statistics are very different for chaotic and nonchaotic well dynamics, we show that the *mean* splittings of differently shaped wells, including integrable and chaotic wells, are the same if their well areas and barrier parameters are the same. We also consider the case of tunneling from a single well into a region with outgoing quantum waves.

DOI: 10.1103/PhysRevE.86.056212 PACS number(s): 05.45.Mt, 73.40.Gk, 03.65.Xp, 03.75.Lm

I. INTRODUCTION

A. Background

According to the correspondence principle, the predictions of quantum and classical mechanics should coincide in the limit of short quantum wavelength. It is particularly interesting to investigate possible manifestations of the correspondence principle in situations where the quantum and classical pictures evidence seemingly different fundamental properties. For example, classical mechanics, being nonlinear, may commonly yield chaos, while quantum mechanics, e.g., as described by the Schrödinger wave equation, is linear and thus cannot yield chaotic dynamics in the usual classical sense (i.e., exponential sensitivity of bounded solutions to small perturbation). Thus, the short wavelength quantum manifestations of chaos in a corresponding classical system has attracted much attention [1], and the study of this issue has been given the appellation *quantum chaos*. In addition to chaos, the quantum phenomenon of tunneling through classically forbidden regions of phase space presents another striking difference between quantum and classical mechanics. In this paper, we investigate short wavelength tunneling from a classically confined region in which the classical orbits are chaotic. Much past work examining the issue of tunneling in classically chaotic systems has been done (e.g., Refs. [2–5] and references therein). For example, one question that has been extensively studied is what happens when a quantum state is initially localized in an integrable region of classical phase space and tunnels through to a chaotic region [2], which is often called dynamical tunneling. In contrast, here, as in Refs. [3–5], we consider the problem of quantum tunneling from a chaotic region through a classical barrier in the absence of an integrable region. While Refs. [3–5] treat this problem in the case of smoothly varying potentials with spatially narrow tunneling paths (e.g., instantons), our concern will be the two-dimensional case where there are piecewise-uniform potentials, long barriers, and confining hard walls [6]. The classical dynamics in this case corresponds to a so-called billiard system. Motivations for considering billiard-type systems include the following: (i) they are potentially realizable in quantum dot contexts and in descriptions of classical optical electromagnetic fields in piecewise-constant dielectrics, (ii) by adjusting the shape of the wells, it is particularly easy to straightforwardly go from integrable to mixed to chaotic phase space, and (iii) comparisons between different shape wells (e.g., between an integrable and a chaotic well) can be made quantitatively precise by keeping certain gross parameters equal (see Sec. I B). With respect to point (iii) above, a major result is that integrable and chaotic cases with the *same* mean splittings differ very greatly in their fluctuation characteristics, with the chaotic case having much smaller splitting fluctuations about the common mean than the integrable case. We believe that, in the billiard case discussed here, point (iii) makes this effect a particularly dramatic instance of a quantum manifestation of classical chaos. We remark that this relative suppression of tunneling fluctuations in the chaotic case occurs because, due to the classical ergodicity of chaotic systems, the quantum states are relatively similar in that they typically effectively spread over the entire classically allowed phase space. In contrast, in integrable systems, due to the existence of extra constants of the motion, different energy states are typically constrained to have much more variation of their distribution in phase space and may avoid the phase space region where tunneling is strongly excited. If so, the tunneling can be exponentially small and very dependent on the particular state. This point, already inherent in the discussions in Refs. [3–5], applies to both the case of billiard-type Hamiltonians and the case of smooth Hamiltonians (e.g., see Fig. 2 of Ref. [3]).

*leemj@umd.edu

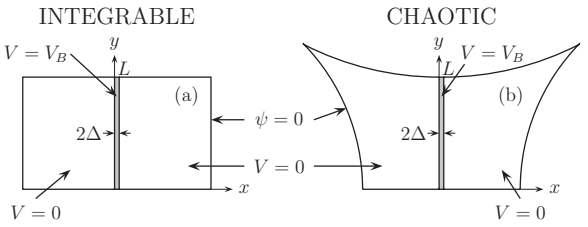

FIG. 1. Symmetrical double wells of area A separated by a tunneling potential barrier of width 2Δ, length L, and height V_B. (a) shows the case of rectangular wells, while (b) shows a case in which all typical orbits are chaotic.

The work presented in this paper is a continuation of a previous work in Ref. [7] in which we reported numerical results and abbreviated heuristic arguments justifying our numerical observations. Our aim now is to provide a fuller theoretical analysis of the results in Ref. [7].

B. Review of the results in Ref. [7]

Reference [7] considers symmetric double-well situations of the type shown in Figs. 1(a) and 1(b). There is a barrier region of uniform potential V_B, width 2Δ, and length L. This barrier region separates two mirror-symmetric wells in which the potential is zero and whose (nonbarrier) boundaries are hard walls. If the energy E is less than V_B, then a point particle is classically confined to one of the wells, and its orbit follows straight lines between specular reflections from the well boundaries (a billiard system). The character of the orbit depends on the shape of the well. For the rectangular well of Fig. 1(a), the orbits of a point particle are integrable, with separately constant horizontal and vertical kinetic energies. For the shape of the well in Fig. 1(b), the convex walls ensure that all typical orbits are chaotic and ergodically fill the full available phase space [7]. In particular, if a typical particle orbit in the Fig. 1(b) billiard is sampled at some random time t, then the location of the particle has a uniform probability density per unit area in the well, and the probability density of the direction of particle motion is uniformly isotropic in $[0,2\pi)$. (Reference [7] also treats other completely regular or chaotic well shapes [8].)

Considering symmetric wells, as in Fig. 1, the quantum eigenstates have either even or odd parity with respect to the center line, and for E sufficiently below the barrier height V_B, we may consider the states to come in symmetric and antisymmetric pairs with nearly equal energies. We denote the σth such pair (E_σ^S, E_σ^A). The symmetric state energy is always less than the antisymmetric state energy, $E_\sigma^S < E_\sigma^A$. The energy level splitting is denoted

$$\Delta E_\sigma = E_\sigma^A - E_\sigma^S. \tag{1}$$

Figure 2 shows as black dots values of ΔE_σ versus $E_\sigma = \frac{1}{2}(E_\sigma^A + E_\sigma^S)$ from numerical solutions of the normalized Schrödinger equation,

$$[\nabla^2 + E - V(x,y)]\psi(x,y) = 0, \tag{2}$$

with $\psi = 0$ on the hard walls, $V = V_B$ in the barrier region $(0 < x < 2\Delta)$, and $V = 0$ in the wells. The parameters V_B, Δ, and L, and the well area A, are all taken to be the same for

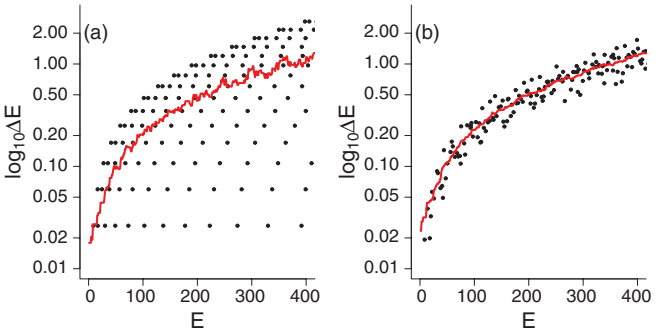

FIG. 2. (Color online) Energy level splittings vs energy plotted as black dots, along with the sliding average (red curve), $\langle \Delta E \rangle_{E,\epsilon}$. The parameters used in the plots are $V_B = 1000$, $\Delta_B = 0.05$, $L = 2.423$, and $A = 4.8$.

the two cases, shown in Figs. 1(a) and 1(b). Also, $EA \gg 1$, i.e., the well dimensions are large compared to the quantum wavelength, corresponding to the semiclassical regime. Shown in Figs. 2(a) and 2(b), by the red curves, is a sliding average $\langle \Delta E \rangle_{E,\epsilon}$ of ΔE_σ using a window, $(E - \epsilon)$ to $(E + \epsilon)$, that encompasses 2 to 15 splitting values. Figure 3 shows the two sliding averages plotted together on the same graph for the integrable case [Fig. 1 (a), blue curve] and the chaotic case [Fig. 1 (b), black curve], along with our theoretical result (red curve) to be derived in Sec. V. The two main conclusions from the numerical results of Ref. [7] are the following:

(1) Fluctuations of the quantum splittings are *very much* larger (note the logarithmic vertical scale) in the integrable well case as compared to the chaotic well case.

(2) For the same gross parameters (A, V_B, Δ, L), the sliding average $\langle \Delta E \rangle_{E,\epsilon}$ versus E is independent of the well shape.

In Ref. [7], it was found that conclusions (1) and (2) hold for all pairs of similarly related chaotic and regular well shapes studied [8].

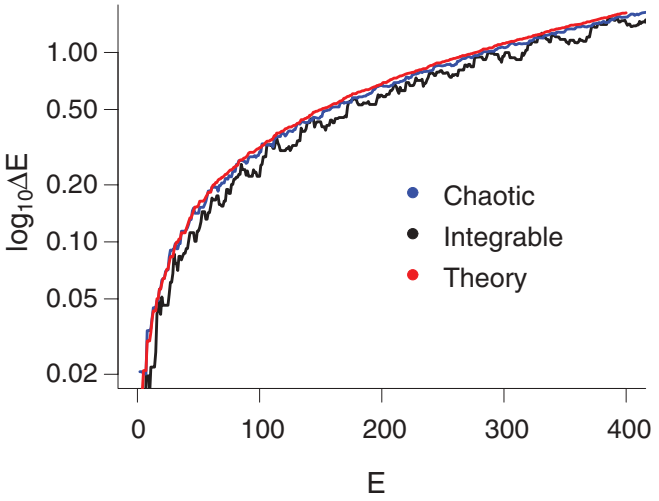

FIG. 3. (Color online) Sliding average vs E. It is seen that the integrable curve is consistently slightly below the other two. We do not have an explanation for this small difference. Perhaps it is a higher order effect ($\sim 1/kL$).

C. Outline

The rest of this paper is organized as follows. Noting that the numerical results in Fig. 2 all satisfy

$$\Delta E_\sigma \ll \tfrac{1}{2}\left(E_{\sigma+1} - E_{\sigma-1}\right), \tag{3}$$

in Sec. II we use perturbation theory to develop a formal expression for ΔE_σ. This expression is essentially Herring's formula [9] adapted to our problem. Section III then applies Berry's random plane wave hypothesis [10] to obtain the statistics of the splittings $\{\Delta E_\sigma\}$ in the case of chaotic classical dynamics. In Sec. IV, as an example, we numerically test the result of Sec. III by comparing its predictions with the data shown in Fig. 2(b). Section V applies a Green's function technique based on the method of Balian and Bloch for deriving the semiclassical perimeter correlation to the density of state for billiard systems [11] to obtain the sliding average splitting $\langle \Delta E \rangle_{E,\epsilon}$ and show that it is independent of well shape. Section VI concludes with further discussion. As discussed in Sec. VI, we report in Appendix B the extension of our method to the treatment of tunneling out of a single chaotic well into an open region with outgoing quantum waves.

II. PERTURBATION THEORY FOR THE STATISTICS OF ENERGY LEVEL SPLITTING FOR CHAOTIC WELLS

A. Setup

We consider the symmetric and antisymmetric wave functions, denoted ψ_S and ψ_A, along with their corresponding energy levels, $E_S \equiv k_S^2$ and $E_A \equiv k_A^2$ [where we choose units in which $\hbar^2/(2m) \equiv 1$]. Referring to Fig. 1, we take the potential to be zero in the left and right wells and to be $V = V_B \equiv k_B^2$ in the barrier region, $0 < x < 2\Delta$. Focusing on the left well, we have that

$$\left(\nabla^2 + k_{S,A}^2\right)\psi_{S,A}^2 = 0 \quad \text{in the left well } (x < 0), \tag{4}$$

$$\left[\frac{\partial}{\partial x}\psi_{S,A}(x,y)\right]_{x=0^-} + \hat{H}_{S,A}[\psi_{S,A}(0^-,y)] = 0, \tag{5}$$

and

$$\psi_{S,A}(x,y) = 0 \tag{6}$$

on the boundary of the left well other than that at $x = 0$. $\hat{H}_S$ and $\hat{H}_A$ denote operators on functions of y that we now obtain.

B. Boundary condition at $x = 0^-$

Within the barrier region, $0 < x < 2\Delta$, ψ_A and ψ_S satisfy the following conditions:

$$\frac{\partial \psi_S}{\partial x} = 0 \text{ and } \psi_A = 0 \text{ at } x = \Delta. \tag{7}$$

Thus, in the barrier, solutions of the time-independent Schrödinger equation,

$$\left[\nabla^2 - \left(k_B^2 - k_{S,A}^2\right)\right]\psi_{S,A} = 0, \quad \psi_{S,A} = 0 \text{ at } y = 0, L, \tag{8}$$

can be written as a linear combination of a symmetric and antisymmetric basis function with coefficient S_m and A_m, i.e.,

$$\psi_S(x,y) = \sum_{m=1}^{\infty} S_m \frac{\cosh\left[\alpha_m(\Delta - x)\right]}{\cosh\left(\alpha_m \Delta\right)} \sin\left(\frac{m\pi y}{L}\right), \tag{9}$$

$$\psi_A(x,y) = \sum_{m=1}^{\infty} A_m \frac{\sinh\left[\alpha_m(\Delta - x)\right]}{\sinh\left(\alpha_m \Delta\right)} \sin\left(\frac{m\pi y}{L}\right), \tag{10}$$

$$\alpha_m = \sqrt{k_B^2 + \left(\frac{m\pi}{L}\right)^2 - k^2}. \tag{11}$$

Noting that both $\psi_{A,S}$ and $\partial\psi_{A,S}/\partial x$ are continuous at $x = 0$, we have that $\hat{H}_S$ and $\hat{H}_A$ in (5) are given by

$$\begin{aligned} \hat{H}_S[f(y)] &\equiv \sum_{m=1}^{\infty} \hat{H}_S^{(m)} f_m \sin\left(\frac{m\pi y}{L}\right), \\ \hat{H}_S^{(m)} &= \alpha_m \tanh\left(\alpha_m \Delta\right), \end{aligned} \tag{12}$$

$$\begin{aligned} \hat{H}_A[f(y)] &\equiv \sum_{m=1}^{\infty} \hat{H}_A^{(m)} f_m \sin\left(\frac{m\pi y}{L}\right), \\ \hat{H}_A^{(m)} &= \alpha_m \coth\left(\alpha_m \Delta\right), \end{aligned} \tag{13}$$

where f_m denote coefficients of the Fourier sine series of $f(y)$,

$$f(y) = \sum_{m=1}^{\infty} f_m \sin\left(\frac{m\pi y}{L}\right). \tag{14}$$

Note also that the $\hat{H}_{S,A}$ operators are self-adjoint,

$$\int_0^L g(y)\hat{H}_{S,A}[f(y)]dy = \int_0^L f(y)\hat{H}_{S,A}[g(y)]dy, \tag{15}$$

where we have assumed that $f(y)$ and $g(y)$ are real.

C. Perturbation expansion

As the thickness of the barrier Δ becomes large, we see from (12) and (13) that $\hat{H}_S$ and $\hat{H}_A$ become the same:

$$\hat{H}_S^{(m)}, \hat{H}_A^{(m)} \to \alpha_m.$$

We denote this limit by the subscript 0 and define a corresponding wave function and energy level, ψ_0 and k_0^2, that satisfy the problem,

$$\left(\nabla^2 + k_0^2\right)\psi_0 = 0 \quad \text{in the left well } (x < 0), \tag{16}$$

$$\left[\frac{\partial}{\partial x}\psi_0(x,y)\right]_{x=0^-} + \hat{H}_0[\psi_0(0^-,y)] = 0, \tag{17}$$

and $\psi_0 = 0$ on the boundaries of the left well other than that at $x = 0$. The operator $\hat{H}_0$ is defined as in Eqs. (12) and (13) with

$$\hat{H}_0^{(m)} = \alpha_m. \tag{18}$$

Since $\hat{H}_S$ and $\hat{H}_A$ become equal as $\Delta \to \infty$, the symmetric and antisymmetric energy eigenfunctions (ψ_S and ψ_A) and energy levels (k_S^2 and k_A^2) also become equal. (In particular, they become ψ_0 and k_0^2.) Thus, for sufficiently large Δ, we can assume that these symmetric and antisymmetric quantities are close to each other and are close to the solution of Eqs. (16)–(18). More formally, if we introduce a small

expansion parameter ϵ, we have

$$\psi_{S,A} - \psi_0 = O(\epsilon), \quad k_{S,A}^2 - k_0^2 = O(\epsilon),$$
$$\hat{H}_{S,A} - \hat{H}_0 = O(\epsilon). \tag{19}$$

Multiplying Eq. (4) by $\psi_0(x,y)dxdy$ and Eq. (16) by $\psi_{S,A}(x,y)dxdy$, integrating over the area of the left well, and subtracting the results, we obtain

$$\int_{LW} [\psi_0 \nabla^2 \psi_{S,A} - \psi_{S,A} \nabla^2 \psi_0] dxdy = \left(k_{S,A}^2 - k_0^2\right) \int_{LW} \psi_0 \psi_{S,A} dxdy, \tag{20}$$

where LW denotes the area of the left well. Applying Green's identity to the left side of this equation, we have essentially Herring's formula [9],

$$\int_0^L \{\psi_0 \hat{H}_{S,A}[\psi_{S,A}] - \psi_{S,A} \hat{H}_0[\psi_0]\}_{x=0} dy = \left(k_{S,A}^2 - k_0^2\right) \int_{LW} \psi_0 \psi_{S,A} dxdy, \tag{21}$$

where we have used the condition that $\psi_{S,A,0} = 0$ on the boundaries of the left well other than that at $x = 0$. Furthermore, from (15), the left side of (21) can be rewritten as

$$\int_0^L \{\psi_0 \Delta \hat{H}_{S,A}[\psi_{S,A}]\}_{x=0} dy = \left(k_{S,A}^2 - k_0^2\right) \int_{LW} \psi_0 \psi_{S,A} dxdy, \tag{22}$$

where $\Delta \hat{H}_{S,A}[f(y)] \equiv \hat{H}_{S,A}[f(y)] - \hat{H}_0[f(y)]$. Noting from (19) that $\Delta \hat{H}_{S,A}$ and $(k_{S,A}^2 - k_0^2)$ are both $O(\epsilon)$, we see that, to lowest order in ϵ, we can set $\psi_{S,A} = \psi_0$ in (22), thus yielding the perturbation theory result,

$$k_{S,A}^2 - k_0^2 = \frac{\int_0^L \{\psi_0 \Delta \hat{H}_{S,A}[\psi_0]\}_{x=0} dy}{\int_{LW} \psi_0^2 dxdy}. \tag{23}$$

It follows from (12), (13), and (18) that $\hat{H}_A^{(m)} > \hat{H}_0^{(m)} > \hat{H}_S^{(m)}$. Thus, we have that $k_A^2 > k_0^2 > k_S^2$. We denote the energy level splitting by $\Delta E = \Delta k^2 \equiv k_A^2 - k_S^2$. Taking the difference between the symmetric and antisymmetric versions of (23) and employing our definitions of $\hat{H}_{S,A,0}$, we obtain

$$\Delta E = \sum_{m=1}^{\infty} \frac{L \alpha_m C_m^2}{\sinh(2\alpha_m \Delta)} \Big/ \int_{LW} \psi_0^2 dxdy, \tag{24}$$

where C_m are the Fourier sine coefficients of $\psi_0(0,y)$,

$$\psi_0(0,y) = \sum_{m=1}^{\infty} C_m \sin\left(\frac{m\pi y}{L}\right). \tag{25}$$

III. EVALUATION OF ΔE FOR CHAOTIC EIGENFUNCTIONS

In the region $x < 0$, but near $x = 0$, the upper well boundary in Fig. 1 is close to $y = L$. Therefore, in this region, we can take

$$\psi_0(x,y) \cong \sum_{m=1}^{\infty} c_m \sin\left(\frac{m\pi y}{L}\right) \sin(k_{x,m} x - \phi_m), \tag{26}$$

where $k_{x,m}^2 = k_0^2 - (m\pi/L)^2$, and ϕ_m is determined by the boundary condition $\partial\psi_0/\partial x = -\hat{H}_0[\psi_0]$ at $x = 0$, which yields

$$\tan\phi_m = \frac{k_{x,m}}{\alpha_m}. \tag{27}$$

Comparing (26) and (25), we see that

$$C_m = -c_m \sin\phi_m, \tag{28}$$

and from (11) and (27), we see that

$$\sin\phi_m = \frac{k_{x,m}}{k_B}. \tag{29}$$

We will view Eq. (26) as in a statistical model and think of the values of the c_m as pseudorandom variables that, for any given two realizations, can be regarded as representing two different eigenfunctions with nearly the same energy k_0^2. In what follows, we will approximate (26) by cutting off the sum at $m = M$, where M is the maximum value of m for which $k_{x,m}^2 > 0$,

$$M = \max\left[m \,\middle|\, k_0 \geqslant \left(\frac{m\pi}{L}\right)\right]. \tag{30}$$

That is, we only include propagating modes.

We now need a model for characterizing the pseudorandom coefficients c_m in (26). To do this, we assume $M \gg 1$, follow Berry [10], and utilize the chaotic classical dynamics of particles in the potential wells, together with the correspondence principle. Our chaotic classical particle trajectories have the following ergodic character: For typical initial conditions and any small localized region δR in the well, a very long orbit will pass through δR many times, and, if one examines these passages, one will find that, as the orbit length approaches infinity, (i) the fraction of time spent by the orbit in the region δR is the ratio of the area of δR to the total area of the well, and (ii) the orientation of the particle's velocity, in its passes through δR, is uniformly distributed in angle. Thus, if we imagine sampling the chaotic orbit at some randomly chosen time, its location will have a uniform probability density distribution in space, and its velocity (whose magnitude is fixed by the particle energy) will have an isotropic probability distribution in its orientation. Thinking of ψ_0^2 as analogous to the classical probability density in space and invoking property (i), the correspondence principle suggests that, for wavelengths that are small compared to the cavity size, the coarse grained average of ψ_0^2 over several wavelengths will have a value that is the same near $x = 0$ as in any other region of the well.

We now ask how the coefficients c_m in (26) are related to the integral $\int_{LW} \psi_0^2 dxdy$ appearing in the denominator of Eq. (24). We see from (26) that the integral of ψ_0^2 over a region of area A_B abutting the barrier and extending not too far away from it is $(A_B/4)\sum c_m^2$, where the factor $1/4$ results from taking the spatial average of $\sin^2(m\pi y/L)\sin^2(k_{x,m}x - \phi_m)$ over several wavelengths. If the wavelength is short, $k_0 L \gg 1$, based on point (i) above and the correspondence principle, one might suppose that this result for $\int_{A_B} \psi_0^2 dxdy$ can be extended to x values far from the barrier. In particular, we expect that the spatial average of ψ_0^2 near $x = 0$ is approximately the same as in any other region of the well. Thus, we obtain the

estimate

$$\int_{LW} \psi_0^2 dxdy \cong \frac{A}{4} \sum_m c_m^2, \tag{31}$$

where (as previously stated) A is the entire area of the left or right well. We expect (31) to hold as long as the barrier dimension L is much greater than a wavelength, $M\pi \approx k_0 L \gg 1$. When the barrier dimension becomes comparable to or smaller than a wavelength, point to point variations in the magnitude of the wave function lead to departures between the average value of ψ_0^2 in the well and the corresponding value near the barrier. However, even if $k_0 L$ is large, Eq. (31) is only approximate, and we expect it to hold with an error that becomes small as $k_0 L \to \infty$. We will find that, when computing fluctuations in energy splittings, the small fluctuating error in (31) can be important (e.g., see Appendix A and Sec. IV). The use of (31) as a strict equality assumes that the coarse grained average of ψ_0^2 is essentially determined throughout the total area, A, by the M amplitudes, C_m of the propagating modes ($k_{x,m}^2 > 0$) near the barrier. This is not always the case. For example, if scars are present, there may be deviation between the average of ψ_0^2 near the barrier and throughout the well. We note that the intensity and frequency of the scarring contribution decreases with increasing $k_0 L$, as shown in Refs. [12,13]. Thus, in the limit $k_0 L \to \infty$, Eq. (31) applies; but the error in (31) depends on the shape of the well. For now, we will proceed on the assumption that the estimate given by Eq. (31) can be used for the denominator of (24). Although we will find that (31) works well for the chaotic shape shown in Fig. 1(b), we will also argue that, in other cases, (31) may not provide as good a model for fluctuations of ΔE.

To invoke property (ii) (i.e., isotropy of velocity direction), we note that the terms in the sum in (26) represent wave propagation directions that make an angle,

$$\theta_m = \arcsin\left(\frac{m\pi}{k_0 L}\right), \tag{32}$$

with respect to the x axis; see Fig. 4.

We imagine that these wave-quantized angles represent a range of the continuous classical angles, where the range for θ_m is

$$\Delta\theta_m = \tfrac{1}{2}(\theta_{m+1} - \theta_{m-1}), \tag{33}$$

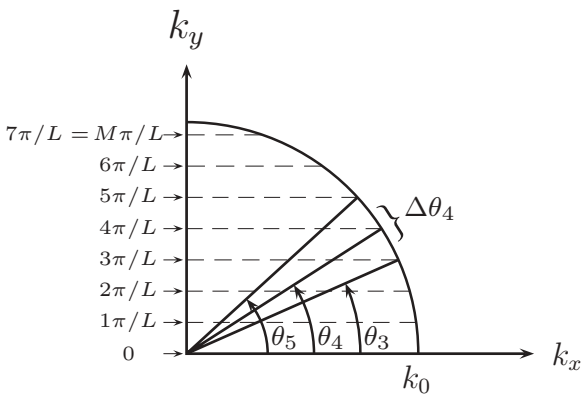

FIG. 4. Propagation directions.

and, for $m = M$, we replace θ_{m+1} by $\pi/2$, while for $m = 1$, we use $\theta_{m-1} = 0$. Invoking the classical orientation isotropy of particle velocities, i.e., point (ii) above, the correspondence principle suggests that $\langle c_m^2 \rangle$ is proportional to $\Delta\theta_m$, $\langle c_m^2 \rangle = (constant)\Delta\theta_m$, where the angle brackets denote an average over our pseudorandom fluctuations. Using this in (31), we obtain

$$\langle c_m^2 \rangle = 4\langle \psi_0^2 \rangle \left(\Delta\theta_m \Big/ \sum_{m'=1}^{M} \Delta\theta_{m'} \right). \tag{34}$$

(Note that the sum over $\Delta\theta_{m'}$ is $(\pi/2) - (\theta_1/2)$, rather than $\pi/2$. We have chosen to omit the angles $0 \leqslant \theta \leqslant \theta_1/2$ because the normally incident wave corresponding to $m = 0$ is ruled out by our boundary condition, $\psi_0 = 0$ at $y = 0, L$ and $x = 0$. In any case, this choice makes only a small difference for $M \gg 1$.) Since we view the c_m as resulting from the sum of many roughly independent classical ray contributions, the central limit theorem implies that c_m will be a Gaussian random variable. Thus, we set

$$c_m = \langle c_m^2 \rangle^{1/2} \xi_m, \tag{35}$$

where ξ_m are independent, Gaussian, zero mean, unit variance random variables,

$$\langle \xi_m \xi_{m'} \rangle = \delta_{m,m'}, \tag{36}$$

with $\delta_{m,m'} = 1$ if $m = m'$, and $\delta_{m,m'} = 0$ if $m \neq m'$.

Combining (31), (35), (34), (29), (28), and (24), we arrive at our main result,

$$\Delta E = \frac{\sum_{m=1}^{M} \mu_m \delta E_m \xi_m^2}{\sum_{m=1}^{M} \mu_m \xi_m^2}, \tag{37}$$

where

$$\delta E_m = \frac{4Lk_{x,m}^2 \alpha_m}{Ak_B^2 \sinh(2\alpha_m \Delta)} \tag{38}$$

is the contribution to the splitting due to the mth mode of the barrier,

$$\mu_m = \frac{2\Delta\theta_m}{\pi - \theta_1} \tag{39}$$

is the weight assigned to the angle θ_m in the well, and the Gaussian random variables ξ_m satisfy (36).

When M is large (i.e., $kL \gg 1$), the number of terms in the sums in (37) is large and the denominator is close to unity with relatively small fluctuations. Although the fluctuations of the denominator from unity are small for large M, it can be necessary to include them, as they significantly contribute to the evaluation of the fluctuations of ΔE from $\langle \Delta E \rangle$, which are also small for large M. As before, the angle brackets $\langle \ldots \rangle$ represent an ensemble average over realizations of the random set $\{\xi_m\}$. The sliding average $\langle \ldots \rangle_{E,\epsilon}$ in Sec. I B is hypothesized to approximate $\langle \ldots \rangle$, if $\langle \ldots \rangle$ is approximately constant over the window width ϵ and if many energy levels are contained in the window.

Equation (37) is a statistical model for the pseudorandom splittings ΔE. This model can be used to generate ensembles of values of ΔE via the Monte Carlo procedure of generating and inserting random values for the Gaussian quantities ξ_m, from which the statistical properties of ΔE can be numerically

determined, as will be illustrated by the example given in Sec. IV.

For large $M \approx kL/\pi$, both the numerator and the denominator in Eq. (37) will have relative fluctuations from their mean values that are small. Recall that the mean of the denominator is, by construction, one. Thus, we expect that replacing the denominator by one (i.e., neglecting denominator fluctuations) will make little difference in the mean value of ΔE obtained from Eq. (37). Fluctuations of the denominator, however, can have a significant effect when looking at fluctuations of ΔE from its mean, as we now discuss. Say the numerator has a large upward (or downward) fluctuation. This might occur because ξ_m^2 for some m values happen to be significantly above (or below) their mean value of one. If this is so, then the denominator will also have a large upward (or downward) fluctuation, and this will mitigate the effect of the numerator fluctuation on ΔE. Thus, the correlation of the fluctuations of the numerator and the denominator reduce the overall fluctuations of ΔE.

We now use Eq. (37) to obtain an expression for the mean value of ΔE in the limit of very large $M \approx kL/\pi$. (In Appendix A, we do an analogous calculation of the variance of ΔE.) Using (37), the expected value of ΔE is

$$\langle \Delta E \rangle = \sum_{m=1}^{M} \mu_m \delta E(\theta_m), \tag{40}$$

where $\delta E(\theta_m) \equiv \delta E_m$, $\delta E(\theta) = (4L)(A\Delta)^{-1} F(\theta)$, and

$$F(\theta) = \cos^2\theta \frac{k_0^2}{k_B^2} \frac{(k_B \Delta \sqrt{1-(k_0/k_B)^2\cos^2\theta})}{\sinh[2k_B\Delta\sqrt{1-(k_0/k_B)^2\cos^2\theta}]}, \tag{41}$$

where we have used $\alpha_m = k_B\sqrt{1-(k_0/k_B)^2\cos^2\theta}$ and $k_m = k_0\cos\theta$. In obtaining (40), we have noted that the denominator of (37) can be written as

$$\sum_{m=1}^{M} \mu_m \xi_m^2 = 1 + \sum_{m=1}^{M} \mu_m (\xi_m^2 - 1), \tag{42}$$

where the second term is a fluctuation [$\langle(\xi_m^2 - 1)\rangle = 0$], which means that each individual eigenstate in the ensemble is not normalized [14,15]. For $M \gg 1$, this fluctuating component is small compared to unity, and we neglect it. (We emphasize, however, that inclusion of this fluctuation can be crucial for a calculation of the variance of ΔE.) In the semiclassical limit $kL \gg 1$, $M \gg 1$, and $\Delta\theta_m$ becomes small, allowing us to approximate the summation over m in (40) by an integral. Thus, (40) becomes

$$\langle \Delta E \rangle = \frac{4L}{A\Delta} I(E/V_B, k_B\Delta), \tag{43}$$

$$I(E/V_B, k_B\Delta) = \frac{2}{\pi}\int_0^{\pi/2} F(\theta) d\theta, \tag{44}$$

and we recall $E/V_B = k_0^2/k_B^2$.

Equation (40) is plotted as the red curve in Fig. 3. We next illustrate the use of (37) by application to the fluctuation data shown in Fig. 2(b).

IV. MONTE CARLO EVALUATION OF ENERGY SPLITTINGS

In order to quantitatively compare our theory with the numerical data for energy level splittings in Fig. 2, we define the sliding average splitting and the sliding average splitting variance as

$$\langle \Delta E \rangle_{E_0,\epsilon} = \frac{1}{N_{E_0,\epsilon}} \sum_{\sigma}^{|E_\sigma - E_0|<\epsilon} \Delta E_\sigma, \tag{45}$$

$$\sigma^2_{\Delta E, E_0, \epsilon} = \frac{1}{N_{E_0,\epsilon}} \sum_{\sigma}^{|E_\sigma - E_0|<\epsilon} (\Delta E_\sigma - \langle \Delta E \rangle_{E_0,\epsilon})^2, \tag{46}$$

where $N_{E_0,\epsilon}$ is the number of states such that $|E_0 - E_\sigma| < \epsilon$ and we choose $\epsilon = \sqrt{E_0}$. This quantity is plotted as a solid line in Figs. 2, 3, and 5. To compare with our result, given by Eq. (37), we use Monte Carlo simulations. At each energy level E_σ plotted in Fig. 2, we use (37) to generate 10 000 splitting values, $\Delta E_{\sigma_i}, i = 1,2,\ldots,10\,000$. Similar to Eq. (45) and (46), for each of the 10 000 sets of Monte Carlo data,

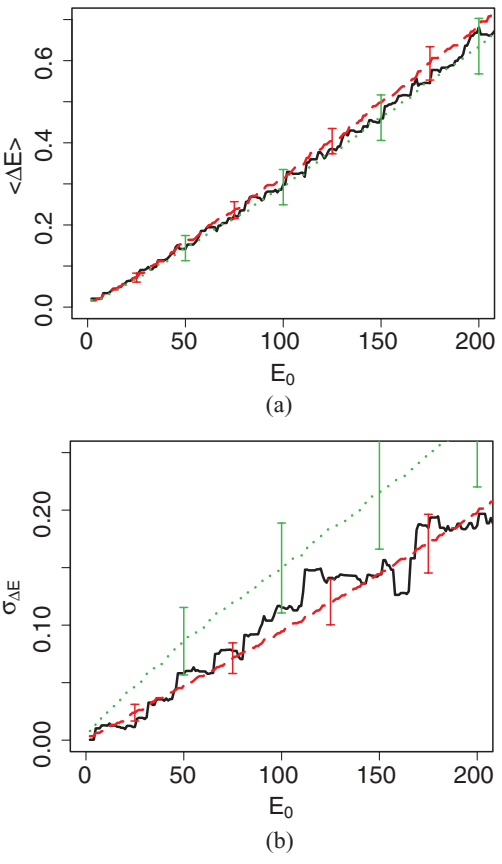

FIG. 5. (Color online) Comparison of (a) sliding average splittings $\langle \Delta E \rangle$ and (b) sliding average splitting variances $\sigma_{\Delta E}$, versus E_0 for numerical data (black), Eq. (37) (red dashed curve), and Eq. (37) with its denominator replaced by one (green dotted curve). The bars at each E_0 are the standard deviations of the sliding average splitting (variances) of $\langle \Delta E \rangle$ and $\sigma_{\Delta E}$ values obtained from 10 000 sets of ΔE vs E_0 scans calculated from Eq. (37) [i.e., the subscript i in Eqs. (47) and (48) scans from $i = 1$ to $i = 10\,000$].

$\{\Delta E_{\sigma_i}\}$, we also calculate sliding average splittings,

$$\langle \Delta E \rangle_{E_0,\epsilon,i} = \frac{1}{N_{E_0,\epsilon}} \sum_{\sigma_i}^{|E_{\sigma_i}-E_0|<\epsilon} \Delta E_{\sigma_i}, \tag{47}$$

and sliding average splitting variances,

$$\sigma^2_{\Delta E,E_0,\epsilon,i} = \frac{1}{N_{E_0,\epsilon}} \sum_{\sigma_i}^{|E_{\sigma_i}-E_0|<\epsilon} (\Delta E_{\sigma_i} - \langle \Delta E \rangle_{E_0,\epsilon,i})^2. \tag{48}$$

At each E_0, we can calculate the ensemble average and variance of the sliding average splitting and the sliding average splitting variance. In Fig. 5, we compare these Monte Carlo results (plotted in red) with results from numerical solutions of the Schrödinger wave equation (plotted in black); we also compare these results to what (37) would predict if the denominator of Eq. (37) were set to unity (plotted in green). Figure 5(a) shows that regardless of whether fluctuations in the denominator are included or neglected, the sliding averages of the splittings for both calculations fall within one ensemble standard deviation of each other, and both agree well with results from the numerical solution of the wave equation. In contrast, we see from Fig. 5(b) that including the fluctuations in the denominator reduces the splitting variance. That is, correlations between the denominator and numerator reduce the estimated eigenfunction to eigenfunction variations in the splitting energy.

To examine the effect of the correlation between the denominator in Eq. (37) and the numerator, we numerically calculate energy splittings for a symmetrical double well that has the same gross parameters (A, V_B, Δ, L) with Fig. 1 but longer wall at $x = 0$ (see Fig. 6) and make analogous figures to Fig. 5 (see Fig. 7). In order to explain the discrepancy in Fig. 7(b) between the theory as expressed by Eq. (37) and our data from the numerical solution of the Schrödinger equation, we now reexamine our assumption that we can use the approximation (31) for $\int_{LW} \psi_0^2 dxdy$ in (37). In particular, as explained in the discussion following Eq. (31), at finite wavelength, $A^{-1}\int_{LW} \psi_0^2 dxdy$ and $A_B^{-1}\int_{A_B} \psi_0^2 dxdy$ may not be perfectly correlated. As an alternate hypothesis, let us now suppose that fluctuations of $A_B^{-1}\int_{A_B} \psi_0^2 dxdy$ are uncorrelated with those of $A^{-1}\int_{LW} \psi_0^2 dxdy$. If this is the case, then the fluctuations of the denominator in Eq. (24) are uncorrelated

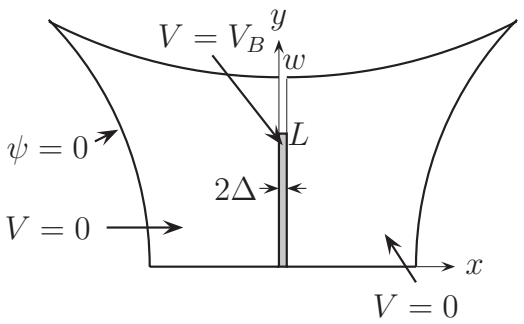

FIG. 6. Symmetrical double wells of area A separated by a non-perfectly-coupled tunneling potential barrier of width 2Δ, barrier length L, height V_B, and wall length w.

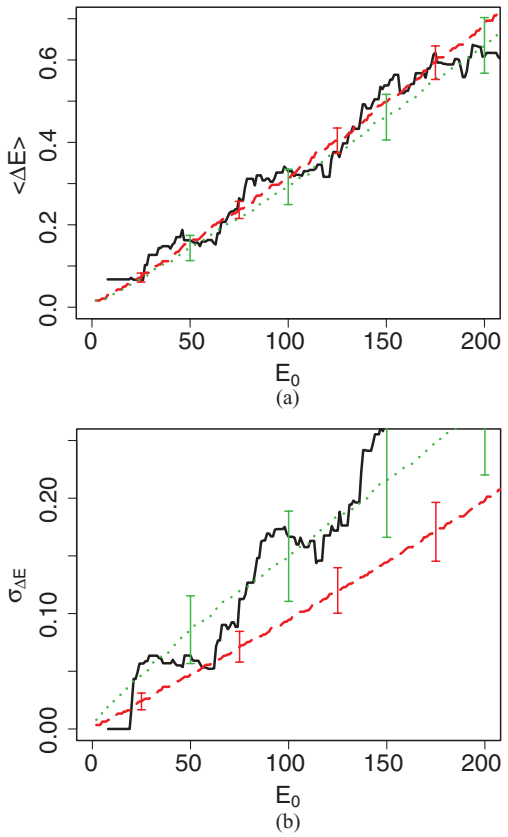

FIG. 7. (Color online) (a) Analogous to Fig. 5(a), but for Fig 6. (b) Analogous to Fig. 5(b), but for Fig 6.

with fluctuations of the numerator. In this situation, we can choose to constrain the denominator to be normalized to one, $\int_{LW} \psi_0^2 dxdy = 1$. In particular, this is consistent with our previous definition $\langle \xi_m^2 \rangle = 1$ and conforms with the idea that $\int_{A_B} \psi_0^2 dxdy$ averaged over many modes should respect the global normalization $\int_{LW} \psi_0^2 dxdy = 1$ for each mode. Thus, this alternate hypothesis yields (37), but with the denominator replaced by one,

$$\Delta E = \sum_{m=1}^{M} \mu_m \delta E_m \xi_m^2. \tag{49}$$

In Appendix C, we provide analytical support for this and show how a transition from the applicability of (37) to the applicability of (49) can take place as a geometrical parameter is varied. Equations (37) and (49) result from two opposite bases, which is a perfect correlation for (37) and zero correlation for (49). As previously discussed in the text following Eq. (37), correlation reduces the fluctuations. Hence, we expect the fluctuation level to lie between the predictions from these two extremes, and we regard the green and red variance curves in Figs. 5(b) and 7(b) as predicted upper and lower bounds for the fluctuation level. Our data for the two chaotic shapes indeed conform to this expectation, where the fluctuation level for the shape in Fig. 1(b) is close to the lower bound, while that for the shape in Fig. 6 is closer to the upper bound.

V. GREEN'S FUNCTION ANALYSIS OF SLIDING AVERAGE OF SPLITTINGS

We have obtained an expression, given by Eq. (40), for the average of the splittings, $\langle \Delta E \rangle$, for chaotic cavities. We have also seen (Fig. 3) that this result agrees numerically with our results for an integrable cavity of rectangular shape. Here we demonstrate in a formal analysis that our result for $\langle \Delta E \rangle$ applies for all cavity shapes independent of whether they are integrable, chaotic, or a mixture of chaotic and integrable in different regions of phase space. Our analysis makes use of a previous work on perimeter corrections to Weyl's equation for the density of states [11].

We begin with the Green's function of the unperturbed left well ($\Delta \to \infty$ in Fig. 1) expanded in orthonormal modes ψ_0^σ of the left well,

$$G_E(\vec{x},\vec{x}') = \sum_\sigma \frac{\psi_0^\sigma(\vec{x})\psi_0^\sigma(\vec{x}')}{E - E_\sigma}, \quad E_\sigma = (k_\sigma)^2, \tag{50}$$

where $(\nabla^2 + E)G_E = \delta(\vec{x} - \vec{x}')$, $(\nabla^2 + E_\sigma)\psi_0^\sigma = 0$ with the appropriate boundary conditions, and $\vec{x} = (x,y)$. According to our perturbation theory [Eq. (23)], the splitting for the unperturbed mode σ is

$$\Delta E_\sigma = \int_0^L \left\{\psi_0^\sigma(x,y)\Delta\hat{H}\left[\psi_0^\sigma(x,y)\right]\right\}_{x=0^-} dy, \tag{51}$$

where the operator $\Delta\hat{H} = \Delta\hat{H}_A - \Delta\hat{H}_S$. Operating on (50) with $\Delta\hat{H}$, and setting $E = E_0 - i\epsilon$, where $\epsilon > 0$, we obtain

$$\begin{aligned} &\mathrm{Im}\int_0^L \{[\Delta\hat{H}G_{E_0-i\epsilon}]_{\vec{x}'=\vec{x}}\}_{x=0^-} dy \\ &\quad = \sum_\sigma \frac{\epsilon}{(E_0 - E_\sigma)^2 + \epsilon^2}\Delta E_\sigma. \end{aligned} \tag{52}$$

For $\epsilon \gg \rho^{-1}(E_0)$, where $\rho^{-1}(E_0)$ is the average spacing between energy levels [$\rho(E_0)$ is the density of states], yet small compared to E_0, the right-hand side of (52) is the product of $\pi\rho(E_0)$ and the Lorentzian sliding average of ΔE_σ. This follows from

$$\sum_\sigma \frac{\epsilon/\pi}{(E_0 - E_\sigma)^2 + \epsilon^2} \cong \rho(E_0) = \frac{A}{4\pi}, \tag{53}$$

where the right-hand equality is Weyl's formula for a well of area A and is independent of E_0 for the two-dimensional case we are treating. Equations (52) and (53) yield the following expression for the sliding average:

$$\langle \Delta E_\sigma \rangle_{E_0,\epsilon} = \frac{4}{A}\mathrm{Im}\left\{\int_0^L [(\Delta\hat{H}G_{E_0-i\epsilon})_{\vec{x}'=\vec{x}}]_{x=0} dy\right\}. \tag{54}$$

For the purpose of evaluating the right-hand side of (54), we consider ϵ to be large enough that waves with energy $E_0 - i\epsilon$ attenuate to negligible values in a distance of the order of the well size. With this stipulation, we can replace $G_{E_0-i\epsilon}$ in Eq. (54) by $G^{(0)}_{E_0-i\epsilon}$, where $G^{(0)}_{E_0-i\epsilon}$ is the Green's function for the case shown in Fig. 8, with outgoing waves as $x \to -\infty$.

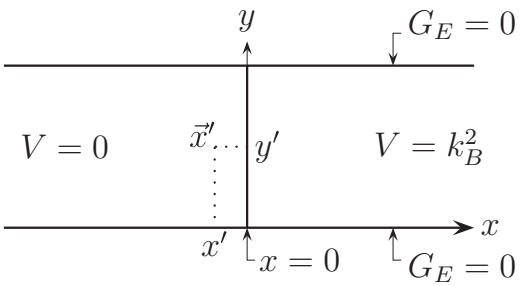

FIG. 8. Geometry for the Green's function.

Making use of the δ function expansions,

$$\delta(x - x') = \frac{1}{2\pi}\int \exp[ik_x(x - x')]dk_x, \tag{55}$$

$$\delta(y - y') = \frac{1}{\pi L}\sum_{m=1}^{\infty} \sin\left(\frac{m\pi y'}{L}\right)\sin\left(\frac{m\pi y}{L}\right), \tag{56}$$

we obtain

$$\begin{aligned} G_E^{(0)} = \frac{1}{\pi L}\int dk_x \sum_{m=1}^{\infty}\Bigg\{&\sin\left(\frac{m\pi y'}{L}\right)\sin\left(\frac{m\pi y}{L}\right) \\ &\times \frac{e^{ik_x(x-x')} + \Gamma_m e^{-ik_x(x+x')}}{E - \left[k_x^2 + \left(\frac{m\pi}{L}\right)^2\right]}\Bigg\}. \end{aligned} \tag{57}$$

Noting that for $x > 0$, the zero order Green's function has the form $G_E^{(0)} = \sum G_m \sin(m\pi y/L)\exp(-\alpha_m x)$, the reflection coefficient Γ_m is determined from the boundary condition,

$$\frac{1}{G_E^{(0)}}\left.\frac{\partial G_E^{(0)}}{\partial x}\right|_{x=0^-} = \frac{1}{G_E^{(0)}}\left.\frac{\partial G_E^{(0)}}{\partial x}\right|_{x=0^+}, \tag{58}$$

which yields

$$\Gamma_m = e^{-2i\phi_m(k_x)}, \tag{59}$$

$$\phi_m(k_x) = \arctan\left(\frac{\alpha_m}{k_x}\right), \tag{60}$$

where

$$\alpha_m = \sqrt{k_B^2 + \left(\frac{m\pi}{L}\right)^2 - E_0}. \tag{61}$$

Inserting (57) into (54), and making use of our results for $\hat{H}_{A,S}$ in Eqs. (12) and (13), we obtain

$$\begin{aligned} \langle \Delta E_\sigma \rangle_{E_0,\epsilon} = \frac{4}{A}\sum_m \int_{-\infty}^{+\infty} dk_x \frac{\epsilon}{\pi}\Bigg\{&\frac{\alpha_m}{\sinh(2\alpha_m\Delta)} \\ &\times \frac{\mathrm{Re}[1 + \Gamma_m(k_x)]}{\left[k_x^2 + \left(\frac{m\pi}{L}\right)^2 - E_0\right]^2 + \epsilon^2}\Bigg\}. \end{aligned} \tag{62}$$

In writing (62), we have neglected $\mathrm{Im}[\Gamma_m(k_x)]$, which will be valid for $E_0 \gg \epsilon$. In this same limit, we may also neglect the

variation of $\Gamma_m(k_x)$ and α_m in the range

$$\epsilon \geqslant \left[k_x^2 + \left(\frac{m\pi}{L}\right)^2 - E_0\right] \geqslant -\epsilon.$$

Thus, we set $k_x = k_{x_0} \equiv \sqrt{E_0 - (m\pi/L)^2}$ and $\alpha_{m_0} = \sqrt{k_B^2 + (m\pi/L)^2 - E_0}$ in (62), yielding

$$\langle \Delta E \rangle = \frac{4}{A} \sum_{m=1}^{M} \frac{\alpha_{m_0}}{k_{x_0}} \frac{\mathrm{Re}[1 + \Gamma_m(k_{x_0})]}{\sinh(2\alpha_{m_0}\Delta)}, \tag{63}$$

where we have cut the sum over m off at M [defined by Eq. (30)] and dropped the subscript E_0,ϵ. Using our result (59) for Γ_m, we finally obtain

$$\langle \Delta E \rangle = \frac{4L}{A\Delta} \sum_{m=1}^{M} \left(\frac{2\Delta\theta}{\pi}\right) \frac{k_{x_0}^2 \alpha_{m_0}}{k_B^2 \sinh(2\alpha_{m_0}\Delta)}, \tag{64}$$

where we have used $\Delta\theta_m = \pi/(k_x L)$, which is valid in the limit $m \gg 1$. This result is the same as our Eq. (40) derived for the chaotic shape, thus demonstrating that it is independent of how the well is shaped, as well as whether the orbits are chaotic, integrable, or mixed.

VI. DISCUSSION AND CONCLUSION

Defining fluctuating weights w_m by

$$w_m = \frac{\xi_m^2 \mu_m}{\sum_{m=1}^{M} \xi_m^2 \mu_m}, \tag{65}$$

Eq. (37) takes the form of a weighted average,

$$\Delta E = \sum_{m=1}^{M} w_m \delta E_m, \tag{66}$$

where δE_m is defined in (38). For the case of rectangular wells, the unperturbed states ($\Delta \to \infty$) are

$$\psi_0(x,y) = \sin\left(\frac{m\pi y}{L}\right) \sin(k_{x,m} x - \phi_m), \tag{67}$$

where m labels the vertical wave number, $k_y = m\pi/L$. The insertion of (67) into the perturbation result (24) yields

$$\Delta E = \delta E_m. \tag{68}$$

Thus, ΔE in the chaotic case is a weighted average over the tunneling rates for the rectangular well. This self-averaging, done by each individual chaotic mode, is responsible for the reduction of the mode-to-mode tunneling fluctuations. The larger the number of m values effectively taking part in the averaging, the lower the fluctuation level. Since this number scales with $M \approx kL/\pi$, we conclude that, as shown in Appendix A, the fluctuation level for splittings in the chaotic case decreases with increasing kL,

$$\frac{\sigma}{\langle \Delta E \rangle} = \frac{\langle (\Delta E - \langle \Delta E \rangle)^2 \rangle^{1/2}}{\langle \Delta E \rangle} \sim (kL)^{-1/2}, \tag{69}$$

and the ratio of the fluctuation level for the chaotic case to that for the integrable case has this same predominant scaling. Thus, the difference between fluctuation levels of the chaotic and integrable cases becomes large with increasing energy (however, if E is increased, V_B may also have to be increased in order to keep E/V_B less than one).

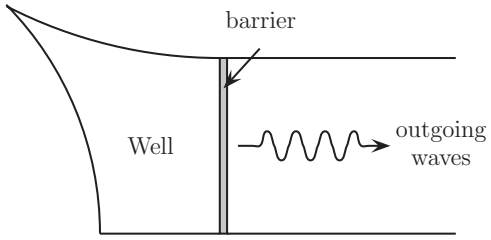

FIG. 9. Tunneling from a single well into an unconfined region.

Equation (66) also provides a simple way of understanding our observation that the sliding averages for the chaotic and rectangular well cases are the same. We first recall that the weights w_m given by (65) have averages corresponding to an isotropic distribution of incident plane waves on the boundary. Furthermore, according to Weyl's law for two-dimensional billiards, the distribution of modes in k space is isotropic and uniform. Thus, if the sliding average for the rectangle includes a sufficient number of modes in the averaging window, then it produces an isotropic averaging, just as in the chaotic case. Thus, as observed in Fig. 3 and demonstrated by the analysis of Sec. V, we expect the chaotic and regular wells to yield the same sliding average.

We remark that, from the experimental point of view, due to the short wavelength necessary for observing semiclassical effects, the symmetry required for realizing splitting statistics may be stringent. Another, much less demanding situation is that of tunneling from a single well into a region of outgoing quantum waves, as pictured in Fig. 9. In this case, the energy levels acquire an imaginary part, $E_\sigma = E_\sigma^{(R)} - i E_\sigma^{(I)}$, where, for $E_\sigma^{(R)} < V_B$ and Δ sufficiently large, $E_\sigma^{(R)} \gg E_\sigma^{(I)}$, so that a perturbation analysis similar to that in Secs. II and III can be applied. The result is that the statistics of the tunneling escape rates $\{E_\sigma^{(I)}\}$ are similar to those for the tunneling-induced splittings $\{\Delta E_\sigma\}$. The statistical model for $\{E_\sigma^{(I)}\}$ [analogous to Eq. (37)] is derived in Appendix B. The result has the same form as that given in Eqs. (65) and (66). Thus, the subsequent discussion, including Eq. (69), also applies for $\{E_\sigma^{(I)}\}$. Hence, the same chaos regularization of tunneling is expected to apply for the escape rates in situations like that shown in Fig. 9.

In conclusion, we have presented a semiclassical analysis of energy level splitting of symmetric, quantum-dot-type, double-well systems, where the wells are separated by a tunneling barrier. Our analysis quantitatively explains the observed mean splittings and their fluctuations. The mean is found to be independent of the well shape and independent of whether the well orbits are chaotic or not. In contrast, the fluctuation statistics are vastly different when the well orbits are integrable, as compared to when they are chaotic, with the chaotic case yielding much-reduced fluctuations when the lateral barrier length is large compared to a wavelength.

ACKNOWLEDGMENTS

This work was supported by ONR (Grants No. N00014-07-1-0734 and No. N000140911190) and by AFOSR (Grant No. FA99500710049).

APPENDIX A: VARIANCE OF THE SPLITTINGS FOR LARGE kL AND LARGE $k_B\Delta$

Here we apply (37) to obtain an analytical expression for the variance of $\{\Delta E_\sigma\}$ for large kL and large $k_B\Delta$. Because of the approximations that we will use, the result will not be applicable for explaining the numerical results in Fig. 2(b), and this is why we used the Monte Carlo procedure in Sec. IV. Nevertheless, this calculation is instructive; e.g., it clearly shows that the splitting variance relative to the mean $\langle\Delta E\rangle$ decreases as $(kL)^{-1}$ for increasing kL (also see the discussion in Sec. VI).

We begin by using (40) and (42) to reexpress (37) as

$$\Delta E = \langle\Delta E\rangle\frac{1+\alpha}{1+\beta}, \tag{A1}$$

where

$$\alpha = \frac{\sum_{m=1}^{M}\mu_m\delta E_m\left(\xi_m^2-1\right)}{\langle\Delta E\rangle}, \tag{A2}$$

$$\beta = \sum_{m=1}^{M}\mu_m\left(\xi_m^2-1\right), \tag{A3}$$

with $\langle\Delta E\rangle$ being the expression given by (40), and $\langle\alpha\rangle = \langle\beta\rangle = 0$ by virtue of $\langle\xi_m^2\rangle = 1$.

Anticipating that α and β are small compared to unity (i.e., $\langle\alpha^2\rangle, \langle\beta^2\rangle \ll 1$), we expand (A1) to obtain

$$\frac{\Delta E - \langle\Delta E\rangle}{\langle\Delta E\rangle} \cong \alpha - \beta. \tag{A4}$$

Squaring (A4) and averaging over realizations of the Gaussian random variables $\{\xi_m\}$ yields the following expression for the variance σ^2:

$$\frac{\sigma^2}{\langle\Delta E\rangle^2} = 2\sum_{m=1}^{M}\mu_m^2\left[\frac{\delta E_m}{\langle\Delta E\rangle}-1\right]^2, \tag{A5}$$

where we have used $\langle(\xi_m^2-1)(\xi_{m'}^2-1)\rangle = 2\delta_{mm'}$. For large M (i.e., large kL), we now attempt to approximate the summation of the right-hand side of (A5) by an integral over θ. For large M and θ_m not too close to $\pi/2$,

$$\mu_m \cong \frac{2}{kL\cos\theta_m}; \tag{A6}$$

see Fig. 4. Using this in (A5), we obtain

$$\frac{\sigma^2}{\langle\Delta E\rangle^2} = 2\int_0^{\theta_*}\frac{2}{kL\cos\theta}\left[\frac{\delta E(\theta)}{\langle\Delta E\rangle}-1\right]^2\frac{d\theta}{\pi/2}. \tag{A7}$$

While the upper limit of the integration in (A7) might nominally be supposed to be $\pi/2$, we have instead replaced it by θ_* because, due to the term $1/\cos\theta$ in the integrand, the integral diverges logarithmically at $\theta_* = \pi/2$. This is an artifact of our approximation (A6), which is not accurate for small $\cos\theta_m$ (e.g., it predicts $\mu_m \to \infty$ as $\theta_m \to \pi/2$). Since the divergence is logarithmic, the size of the contribution to the variance from the vicinity of θ near $\pi/2$ can be roughly estimated by appropriately cutting off the integral at θ_* slightly below $\pi/2$. Based on the construction shown in Fig. 10, we

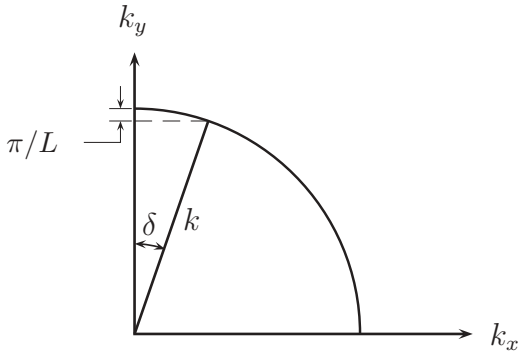

FIG. 10. For $kL/\pi \ll 1$, the angle $\delta \cong \sqrt{2\pi/kL}$.

choose as an appropriate cutoff

$$\theta_* = \frac{\pi}{2} - \sqrt{\frac{2\pi\gamma}{kL}}, \tag{A8}$$

where γ is of the order of one. The result will be insensitive to a precise choice of γ. The contribution from θ near $\pi/2$ is then estimated to be of the order of

$$\frac{1}{kL}\ln\left(\frac{kL}{2\pi\gamma}\right), \tag{A9}$$

where we obtain this result by approximating $\cos\theta$ by $(\pi/2-\theta)$ setting $\theta = \pi/2$ in $\delta E(\theta)$, and noting from Eq. (41) that $\delta E(\pi/2) = 0$.

We now argue that, in an appropriate parameter regime, the contribution (A9) is dominated by the contribution to the integral from the vicinity of $\theta = 0$. In particular, for $k_B\Delta$ sufficiently large,

$$\frac{\delta E(0)}{\langle\Delta E\rangle} \gg 1. \tag{A10}$$

For $\theta^2 \ll 1$, Eqs. (41)–(51) yield

$$\left[\frac{\delta E(\theta)}{\langle\Delta E\rangle}\right]^2 \cong \left(\frac{16}{\pi}\right)\nu\exp\left(-2\nu\theta^2\right), \tag{A11}$$

where

$$\nu = \frac{k_B\Delta}{\sqrt{1-(k/k_B)^2}}. \tag{A12}$$

For example, for future reference we regard (A10) to be satisfied for $\nu \gtrsim 5$. Using (A10) and (A11) in (A7), we obtain:

$$\frac{\sigma^2}{\langle\Delta E\rangle^2} \cong \frac{64}{\pi}\sqrt{\frac{\nu}{2\pi}}\frac{1}{kL}. \tag{A13}$$

Comparing (A13) and (A9), we see that (A13) is larger than (A9) for $\nu \sim 5$ if

$$16 \gtrsim \ln\left(\frac{kL}{2\pi}\right) = \ln\left(\frac{L}{\lambda}\right), \tag{A14}$$

where $\lambda = 2\pi/k$. Thus, we conclude from (A14) that, even when L is many wavelengths λ, the log contribution, given by (A9), is not significant and the predominant scaling of σ is as in (A13),

$$\frac{\sigma}{\langle\Delta E\rangle} \sim (kL)^{-1/2}. \tag{A15}$$

APPENDIX B: ESCAPE RATE FROM A CHAOTIC WELL TO AN OPEN REGION

In this Appendix, we outline the analysis of the situation illustrated in Fig. 9. Again taking $x = 0$ to coincide with the left face of the barrier, 2Δ to be the barrier width, and L to be the vertical dimension of the barrier boundary, we write $\psi(x,y)$ in $x \geqslant 2\Delta$ and $0 \leqslant x \leqslant 2\Delta$, respectively, as

$$\psi(x,y) = \sum_{m=1}^{\infty} D_m \sin\left(\frac{m\pi y}{L}\right) e^{ik_{x,m}x}, \tag{B1}$$

$$\psi(x,y) = \sum_{m=1}^{\infty} (E_m e^{-\alpha_m x} + F_m e^{\alpha_m x}) \sin\left(\frac{m\pi y}{L}\right), \tag{B2}$$

where

$$k_{x,m} = \sqrt{E - \left(\frac{m\pi}{L}\right)^2} \quad \text{for } E \geqslant \left(\frac{m\pi}{L}\right)^2, \tag{B3}$$

$$k_{x,m} = i\sqrt{\left(\frac{m\pi}{L}\right)^2 - E} \quad \text{for } E \leqslant \left(\frac{m\pi}{L}\right)^2, \tag{B4}$$

$$\alpha_m = \sqrt{\left(\frac{m\pi}{L}\right)^2 + V_B - E}, \quad V_B > E. \tag{B5}$$

Applying the continuity of ψ and $\partial\psi/\partial x$ at $x = 2\Delta$ and at $x = 0$, we obtain the boundary condition at $x = 0^-$,

$$\left[\frac{\partial\psi(x,y)}{\partial x}\right]_{x=0^-} + \hat{H}[\psi(0^-,y)] = 0, \tag{B6}$$

where $\hat{H}$ is defined in a manner analogous to Eqs. (12)–(14) with

$$\hat{H}^{(m)} = \alpha_m \frac{(\alpha_m - ik_m) - (\alpha_m + ik_m)\exp(-4\alpha_m\Delta)}{(\alpha_m - ik_m) + (\alpha_m + ik_m)\exp(-4\alpha_m\Delta)}. \tag{B7}$$

Proceeding as in Sec. II C, perturbation theory gives

$$E - E_0 = \frac{\int_0^L \{\psi_0 \Delta\hat{H}[\psi_0]\}_{x=0^-} dy}{\int_{LW} \psi_0^2 dxdy}, \tag{B8}$$

where $E = E^{(R)} - iE^{(I)}$, $\Delta\hat{H} = \hat{H} - \hat{H}_0$, and $\hat{H}_0$ is defined by (18). Taking the imaginary part of Eq. (B8), we obtain an expression for the tunneling rate,

$$E^{(I)} = -\frac{\int_0^L \{\psi_0 \mathrm{Im}(\Delta\hat{H}[\psi_0])\}_{x=0^-} dy}{\int_{LW} \psi_0^2 dxdy}. \tag{B9}$$

Assuming that $\exp(-4\alpha_m\Delta)$ is small, we find that

$$\mathrm{Im}\left(\hat{H}^{(m)} - \hat{H}_0^{(m)}\right) \approx -\frac{4}{V_B}\alpha_m^2 k_{x,m}\exp(-4\alpha_m\Delta), \tag{B10}$$

which yields

$$E^{(I)} = \frac{2L}{V_B}\frac{\sum_m C_m^2 \alpha_m^2 k_{x,m}\exp(-4\alpha_m\Delta)}{\int_{LW}\psi_0^2 dxdy}, \tag{B11}$$

where (B11) is analogous to (24). We can now easily parallel the steps of Sec. III that lead to Eq. (37). Indeed, comparing (B11) and (24), we can obtain (B11) from (24) by making the following replacement in (24):

$$\frac{1}{\sinh 2\alpha_m\Delta} \longrightarrow \frac{2}{V_B}\alpha_m k_{x,m}\exp(-4\alpha_m\Delta). \tag{B12}$$

Using the replacement (B12) in Eq. (37), we obtain the following statistical model for the tunneling rates from a chaotic well to an open region:

$$E^{(I)} = \sum_{m=1}^{M} w_m E_m^{(I)}, \tag{B13}$$

where

$$E_m^{(I)} = \frac{8Lk_{x,m}^3\alpha_m^2\exp(-4\alpha_m\Delta)}{AV_B^2}, \tag{B14}$$

and w_m is as defined in Eq. (65). Note that Eq. (B13) has the same form as Eq. (66).

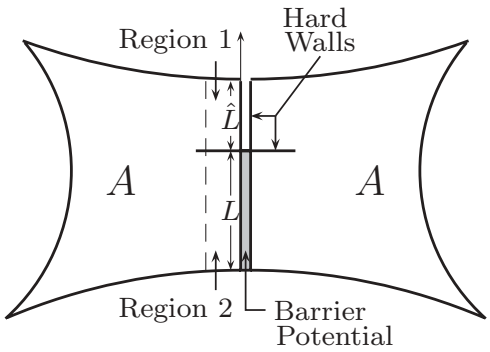

FIG. 11. Model billiard for the analysis in Appendix C.

APPENDIX C: MODEL FOR THE UPPER AND LOWER BOUNDS ON THE SPLITTING VARIANCE

In this Appendix, we consider a model which is similar to that in Fig. 6, but with a modification that will facilitate analysis. This model is shown in Fig. 11. The main feature of this model is the addition of a horizontal, hard, thin septum a distance L from the bottom of the center of the billiard. This septum separates the region near the vertical part of the well boundary abutting the potential barrier (labeled Region 2 in the figure) from that abutting the vertical hard wall well boundary segment (labeled Region 1 in the figure). Using this model, we now present an analysis supporting our claim that as the parameter $L/(L + \hat{L})$ ($\hat{L}$ is defined in Fig. 11) varies from 1 to 0, the splitting variance $\sigma_{\Delta E}^2$ transitions from the lower bound, given by Eq. (49), to the upper bound, given by Eq. (37).

Applying the random plane wave hypothesis to Region 2, we model the statistics of the spatial averages over Region 2 of ψ_0^2 for given modes as

$$\left(\bar{\psi_0^2}\right)_2 = \sum_{m=1}^{M} \mu_m \xi_m^2, \quad M = \mathrm{Int}\left(\frac{kL}{\pi}\right), \tag{C1}$$

where the overbar denotes the spatial average, $\sum_{m=1}^{M}\mu_m = 1$, ξ_m are independent and identically distributed Gaussian variables,

$$\langle \xi_m \xi_{m'} \rangle = \langle \xi^2 \rangle \delta_{mm'}, \tag{C2}$$

and a given random realization of the ξ_m is hypothesized to statistically model a given mode. Doing the same thing for Region 1, we model the statistics of spatial averages of ψ_0^2 over Region 1 for given modes as

$$\left(\bar{\psi}_0^2\right)_1 = \sum_{\hat{m}=1}^{\hat{M}} \hat{\mu}_{\hat{m}} \hat{\xi}_{\hat{m}}^2, \quad \hat{M} = \mathrm{Int}\left(\frac{k\hat{L}}{\pi}\right), \tag{C3}$$

with a similar definition of $\hat{\mu}_{\hat{m}}$ and $\hat{\xi}_{\hat{m}}$. Averaging over many modes (such averages are denoted $\langle \cdots \rangle$), we get

$$\left\langle \left(\bar{\psi}_0^2\right)_2 \right\rangle = \langle \xi^2 \rangle, \quad \left\langle \left(\bar{\psi}_0^2\right)_1 \right\rangle = \langle \hat{\xi}^2 \rangle. \tag{C4}$$

Since we expect the model averages of ψ_0^2 over any region to be the same, $\langle \xi^2 \rangle = \langle \hat{\xi}^2 \rangle$, and we define $\langle \xi^2 \rangle = \langle \hat{\xi}^2 \rangle = 1$.

We now adapt the additional model hypothesis of perfect, mode by mode, correlation between the average of ψ_0^2 over the whole region A and its average over the combined area of Region 1 plus Region 2. While this may not really apply, it should yield a valid qualitative model for the issue that we wish to study. This gives

$$\left(\bar{\psi}_0^2\right)_A = \frac{L}{L+\hat{L}} \left(\bar{\psi}_0^2\right)_2 + \frac{\hat{L}}{L+\hat{L}} \left(\bar{\psi}_0^2\right)_1, \tag{C5}$$

where

$$\frac{L}{(L+\hat{L})} = \frac{\text{Area of Region 2}}{\text{Area of Regions 1} + 2}. \tag{C6}$$

Letting $r \equiv L/(L+\hat{L})$ and following our previous work, the application of Herring's formula gives

$$\frac{\Delta E}{\langle \Delta E \rangle} = \frac{1+\alpha}{1 + r\beta + (1-r)\gamma}, \tag{C7}$$

where

$$\alpha = \sum_{m=1}^{M} \mu_m \frac{\delta E_m}{\langle \Delta E \rangle} \left(\xi_m^2 - 1\right), \quad \beta = \sum_{m=1}^{M} \mu_m \left(\xi_m^2 - 1\right),$$

$$\gamma = \sum_{\hat{m}=1}^{\hat{M}} \hat{\mu}_{\hat{m}} \left(\hat{\xi}_{\hat{m}}^2 - 1\right), \quad \langle \alpha \rangle = \langle \beta \rangle = \langle \gamma \rangle = 0.$$

Expanding for small $\alpha \sim \beta \sim \gamma \ll 1$, we obtain the following expression for the normalized splitting fluctuation δ:

$$\delta \equiv \frac{\Delta E - \langle \Delta E \rangle}{\langle \Delta E \rangle} \cong \alpha - r\beta + (1-r)\gamma. \tag{C8}$$

The normalized splitting variance is thus

$$\langle \delta^2 \rangle \cong \langle \alpha^2 \rangle - 2r\langle \alpha\beta \rangle r^2 \langle \beta^2 \rangle + (1-r)^2 \langle \gamma^2 \rangle,$$

where we have used $\langle \alpha\gamma \rangle = \langle \beta\gamma \rangle = 0$, reflecting the assumption that $\langle \xi_m \hat{\xi}_{\hat{m}} \rangle = 0$ for all m and $\hat{m}$.

Say we keep k, L, and A fixed and vary $\hat{L}$, which is equivalent to keeping α and β fixed and varying r. How does $\langle \delta^2 \rangle$ change as r varies?

From Eq. (A9) of Appendix A,

$$\frac{\langle \gamma^2 \rangle}{\langle \beta^2 \rangle} = \frac{L}{\hat{L}} \frac{\ln(k\hat{L}/2\pi\gamma)}{\ln(kL/2\pi\gamma)}. \tag{C9}$$

Thus, for $kL \sim k\hat{L} \gg 1$, we have $\langle \gamma^2 \rangle \cong (L/\hat{L})\langle \beta^2 \rangle$, which, when used in our expression for $\langle \gamma^2 \rangle$, gives

$$\langle \delta^2 \rangle = r\langle (\alpha-\beta)^2 \rangle + (1-r)\langle \alpha^2 \rangle, \quad 1 \geqslant r \geqslant 0. \tag{C10}$$

Thus, $\langle \delta^2 \rangle$ varies linearly from its largest value, $\langle \alpha^2 \rangle$ at $r = 0$ [corresponding to Eq. (49)], to its smallest value, $\langle (\alpha-\beta)^2 \rangle$ at $r = 1$ [corresponding to Eq. (37)].

[1] F. Haake, *Quantum Signature of Chaos*, 2nd ed. (Springer-Verlag, New York, 2001); M. C. Gutzwiller, *Chaos in Classical and Quantum Mechanics* (Springer-Verlag, New York, 1990); H.-J. Stöckmann, *Quantum Chaos: An Introduction* (Cambridge University Press, Cambridge, 1999); R. Blumel and W. P. Reinhardt, *Chaos in Atomic Physics* (Cambridge University Press, Cambridge, 1997); E. Ott, *Chaos in Dynamical Systems*, 2nd ed. (Cambridge University Press, Cambridge, 2002), Chap. 11.

[2] M. J. Davis and E. J. Heller, J. Chem. Phys. **75**, 246 (1981); J. D. Hanson, E. Ott, and T. M. Antonsen, Phys. Rev. A **29**, 819 (1984); T. Geisel, G. Radons, and J. Rubner, Phys. Rev. Lett. **57**, 2883 (1986); W. A. Lin and L. E. Ballentine, *ibid.* **65**, 2927 (1990); O. Bohigas, S. Tomsovic, and D. Ullmo, *ibid.* **64**, 1479 (1990); Phys. Rep. **223**, 43 (1993); S. Tomsovic and D. Ullmo, Phys. Rev. E **50**, 145 (1994); E. Doron and S. D. Frischat, Phys. Rev. Lett. **75**, 3661 (1995); D. A. Steck, W. H. Oskay, and M. G. Raizen, Science **293**, 274 (2001); M. Sheinman, S. Fishman, I. Guarneri, and L. Rebuzzini, Phys. Rev. A **73**, 052110 (2006); S. Löck, A. Bäcker, R. Ketzmerick, and P. Schlagheck, Phys. Rev. Lett. **104**, 114101 (2010).

[3] M. Wilkinson and J. Hannay, Physica D **27**, 201 (1987).

[4] S. C. Creagh and N. D. Whelan, Phys. Rev. Lett. **77**, 4975 (1996); **82**, 5237 (1999); Ann. Phys. **272**, 196 (1999).

[5] S. C. Creagh and N. D. Whelan, Phys. Rev. Lett. **84**, 4084 (2000).

[6] In contrast with the billiard-type classical chaos that we treat, smooth Hamiltonians typically yield mixed phase spaces with coexisting chaotic and regular regions. In fact, we are aware of only one instance where a smooth Hamiltonian system has been claimed to be fully chaotic, namely, the anisotropic Kepler problem with zero angular momentum; see M. C. Gutzwiller, Phys. Rev. Lett. **45**, 150 (1980).

[7] L. M. Pecora, H. Lee, D.-H. Wu, T. Antonsen, M.-J. Lee, and E. Ott, Phys. Rev. E **83**, 065201 (2011).

[8] These include the stadium billiard, which, although chaotic due to its continuous family of neutrally stable, "bouncing-ball" periodic orbits, exhibits scar-type modes with tunneling rates that can substantially deviate from the mean. Note that, due to its convex walls, such orbits are absent in the strongly chaotic case of Fig. 1(b).

[9] C. Herring, Rev. Mod. Phys. **34**, 631 (1962).

[10] M. V. Berry, J. Phys. A **10**, 2083 (1977).

[11] R. Balian and C. Bloch, Ann. Phys. **60**, 401 (1970); **63**, 592 (1971); **64**, 271 (1971); R. E. Prange, E. Ott, T. M. Antonsen, B. Georgeot, and R. Blümel, Phys. Rev. E **53**, 207 (1996).

[12] M. V. Berry, Proc. R. Soc. London A **423**, 219 (1989).

[13] T. M. Antonsen, E. Ott, Q. Chen, and R. N. Oerter, Phys. Rev. E **51**, 111 (1995).

[14] J. D. Urbina and K. Richter, Eur. Phys. J. Spec. Top. **145**, 255 (2007).

[15] A potential avenue for future elucidation of such fluctuations might be to employ Bogomolny's semiclassical Green's function approach; see E. Bogomolny, Physica D (Amsterdam, Neth.) **31**, 169 (1988); an example where this approach has been employed in another context is D. Ullmo, S. Tomsovic, and A. Bäcker, Phys. Rev. E **79**, 056217 (2009).